Ambipolar Surface Conduction in Ternary Topological Insulator $Bi_2(Te_{1-x}Se_x)_3$ Nanoribbons

ZhenHua Wang,[†,‡] Richard L. J. Qiu,[‡] Chee Huei Lee,[‡] ZhiDong Zhang,[†] and Xuan P. A. Gao[‡,*]

[†]Shenyang National Laboratory for Materials Science, Institute of Metal Research, and International Centre for Materials Physics, Chinese Academy of Sciences, 72 Wenhua Road, Shenyang 110016, People's Republic of China and [‡]Department of Physics, Case Western Reserve University, Cleveland, Ohio 44106, United States

ABSTRACT

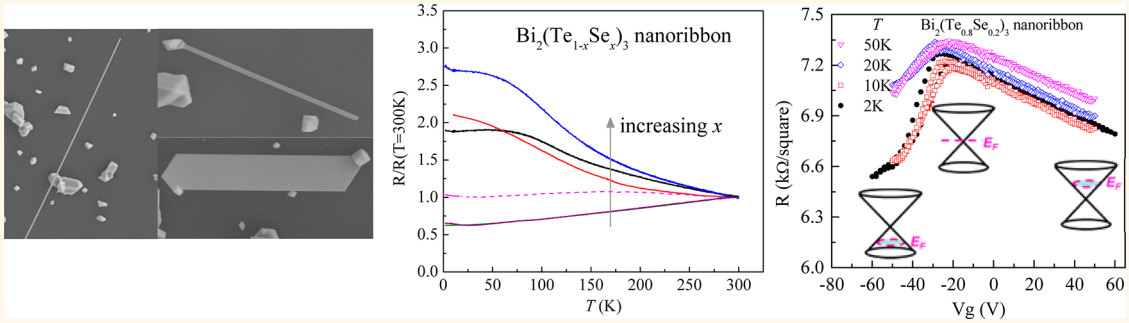

We report the composition- and gate voltage-induced tuning of transport properties in chemically synthesized $Bi_2(Te_{1-x}Se_x)_3$ nanoribbons. It is found that increasing Se concentration effectively suppresses the bulk carrier transport and induces semiconducting behavior in the temperature-dependent resistance of $Bi_2(Te_{1-x}Se_x)_3$ nanoribbons when x is greater than ~10%. In $Bi_2(Te_{1-x}Se_x)_3$ nanoribbons with $x \approx 20\%$, gate voltage enables ambipolar modulation of resistance (or conductance) in samples with thicknesses around or larger than 100 nm, indicating significantly enhanced contribution in transport from the gapless surface states.

KEYWORDS: topological insulator · ambipolar conduction · nanoribbon · bismuth selenide · bismuth telluride

Three-dimensional (3D) topological insulators (TIs) with both metallic surface states and insulating bulk states have attracted enormous research attention. The metallic surface states in 3D TIs consist of a single Dirac cone at the Γ point, which gives rise to interesting surface transport phenomena.[1−3] Binary topological insulators Bi_2Te_3, Bi_2Se_3, and Sb_2Te_3 have been confirmed to have robust surface states by surface-sensitive probes such as angle-resolved photoemission spectroscopy (ARPES)[4−7] and scanning tunneling microscopy/spectroscopy (STM/STS).[8,9] The charge carriers originating from surface states also have been identified by magneto-transport experiments.[10−14] In addition, electrical gating was used as a means to manipulate the gapless surface-state conduction in 3D TIs in Bi_2Te_3 and Bi_2Se_3.[13,15−18] However, the topological surface contribution in transport is hindered by residual bulk carriers from environmental doping or crystal defects.[10,19,20] Therefore, to exploit the surface transport properties of topological insulators, it is crucial to achieve a bulk-insulating state in a topological insulator material.

Recently, ternary and quaternary topological insulators have been synthesized to maximize the surface properties. Shubnikov–de Haas (SdH) oscillations coming from the surface states were observed in bulk $Bi_{2-x}Sb_xSe_3$,[10] Cd-doped Bi_2Se_3,[21] and Bi_2Te_2Se crystals[22] and nanoplates.[23] However, no SdH oscillation was observed in $Bi_{2-x}Ca_xSe_3$[24] due to the disorder from the low-level substitution of Ca^{2+} for Bi^{3+}. Bi_2Te_2Se presented a high resistivity and a variable-range hopping behavior, which is crucial to achieve the surface transport properties.[22] Cd-doped Bi_2Se_3 showed a transition from n-type to p-type

* Address correspondence to xuan.gao@case.edu.

Received for review October 9, 2012 and accepted February 27, 2013.

Published online February 27, 2013
10.1021/nn304684b

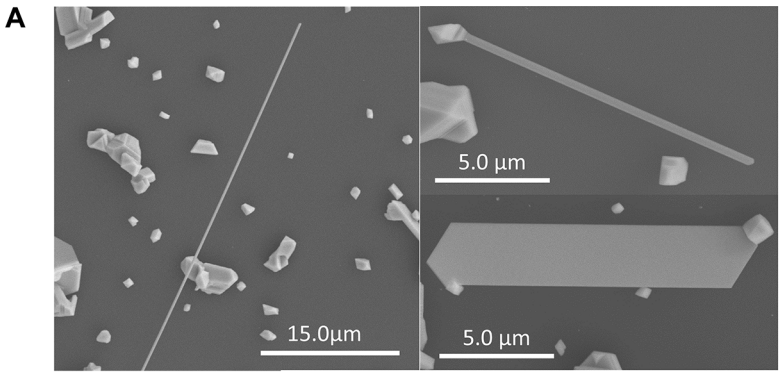

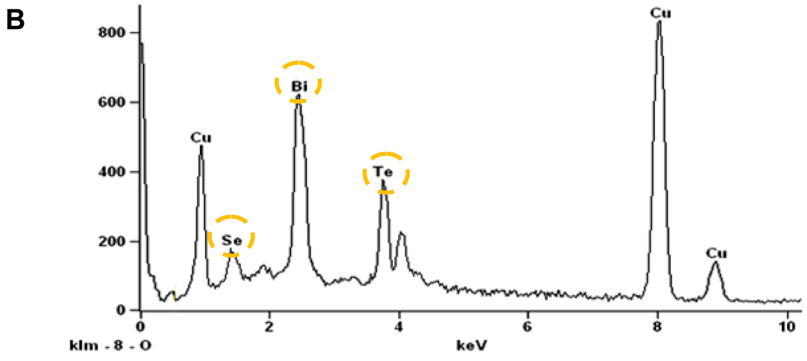

Element Line	Weight %	Weight % Error	Atom %	Atom % Error
Cu K	57.32	+/- 0.74	76.46	+/- 0.99
Se K	3.07	+/- 0.74	3.30	+/- 0.79
Te L	16.16	+/- 0.75	10.73	+/- 0.50
Bi M	23.45	+/- 0.65	9.51	+/- 0.26
Total	100.00		100.00	

Figure 1. Morphological and composition data of $Bi_2(Te_{1-x}Se_x)_3$ nanoribbons. (A) SEM images of $Bi_2(Te_{1-x}Se_x)_3$ nanoribbons with lengths from several μm to tens of μm and widths from several hundred nm to several μm. (B) EDS data of a $Bi_2(Te_{1-x}Se_x)_3$ nanoribbon with $x \approx 20 \pm 5\%$. The Cu peaks originated from the Cu thin film substrate.

conversion upon increasing Se vacancies by postannealing.[21] The solid solution $Bi_{2-x}Sb_xTe_{3-y}Se_y$ showed a series of "intrinsic" compositions and presented a maximally bulk-insulating behavior, which can achieve a surface-dominated transport.[25,26] The SdH oscillation of both Dirac holes and electrons was observed in the compound $Bi_{1.5}Sb_{0.5}Te_{1.7}Se_{1.3}$.[26] Besides studies on bulk materials, topological insulator nanoribbons and nanoplates are expected to have significantly enhanced surface conduction because of their large surface-to-volume ratios.[11] $(Bi_xSb_{1-x})_2Te_3$ nanoplates with a thickness less than 10 nm have been shown to exhibit ambipolar field effect.[27] Alternatively, the Fermi level of Bi_2Te_3 nanoplates could be tuned by Na doping, and enhanced surface-state conduction was observed, in which the ambipolar surface transport could be achieved by applying a back-gate voltage.[28] $Bi_2(Se_xTe_{1-x})_3$ is a topological insulator for all atomic ratios x, similar to $(Bi_xSb_{1-x})_2Te_3$.[27,29,30] In $Bi_2(Se_xTe_{1-x})_3$ nanoribbons and nanoplates with high carrier density, two-dimensional (2D) weak antilocalization was clearly observed.[30] A similar 2D weak antilocalization effect was also observed in Bi_2Te_2Se nanoplates.[31] However, an ambipolar field effect has never been reported in the ternary $Bi_2(Se_xTe_{1-x})_3$ TI materials. Here, we report the synthesis and transport studies of $Bi_2(Te_{1-x}Se_x)_3$ nanoribbons. For nanoribbons with thicknesses of ~100−300 nm, we show that increasing the Se concentration, x, gradually tunes the material from metallic to semiconducting. Moreover, ambipolar field effect from surface-state conduction was achieved by applying a back-gate voltage for a semiconducting compound with $x \approx 20\%$. The thickness of nanoribbons is also found to be important for observing an enhanced ambipolar field effect.

RESULTS AND DISCUSSION

A vapor−liquid−solid (VLS) process was used to synthesize $Bi_2(Te_{1-x}Se_x)_3$ nanoribbons in a vapor transport setup (see Methods section). Figure 1A shows scanning electron microscope (SEM) images of the as -synthesized ribbons, the length of the ribbons ranges from several μm to tens of μm, and the width ranges from a few hundred nm to a few μm. The wide ribbons display 120° facet angles, reflecting the crystal structure. The concentrations of Bi, Te, and Se in $Bi_2(Te_{1-x}Se_x)_3$ nanoribbons were estimated by energy-dispersive X-ray spectroscopy (EDS) on individual nanoribbons. An

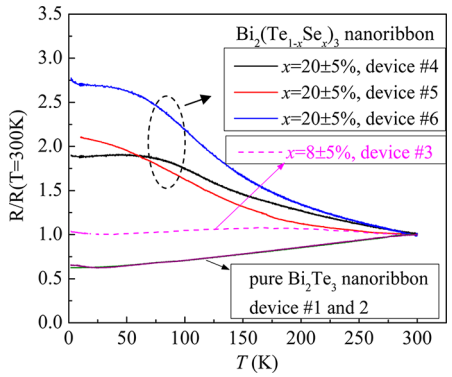

Figure 2. Composition-tuned temperature-dependent transport in $Bi_2(Te_{1-x}Se_x)_3$ nanoribbons. The dependence of resistance on temperature showing the transport property changes from metallic into semiconducting as the concentration of Se increases in $Bi_2(Te_{1-x}Se_x)_3$ nanoribbons. The resistances at 300 K are 0.077, 0.97, 4.44, 6.12, 49.2, and 4.3 kΩ for devices #1−6.

example of EDS data corresponding to a $Bi_2(Te_{1-x}Se_x)_3$ nanoribbon with $x = 20 \pm 5\%$ is shown in Figure 1B. To investigate the transport properties and explore the topological surface conduction in $Bi_2(Te_{1-x}Se_x)_3$ nanoribbons, back-gated field effect transistor (FET) devices were fabricated on doped Si substrates with 300 nm thick SiO_2 on the surface and measured in a cryostat (see Methods section).[14]

Temperature-dependent resistance measurements of $Bi_2(Te_{1-x}Se_x)_3$ nanoribbons with different x show that substituting Te with Se can indeed suppress the residual bulk carriers and tune the Fermi level into the bulk band gap, in a similar way to the studies in bulk crystals.[25] In Figure 2, we compare R *vs* T for a series of $Bi_2(Te_{1-x}Se_x)_3$ nanoribbons with different x. To compare the temperature dependence directly, the resistances of different samples are normalized by the values at 300 K. A clear trend can be seen in Figure 2 that as more Se is incorporated into the Bi_2Te_3, the material turns from metallic into semiconducting at $x > \sim 10\%$. Atomic force microscope (AFM) measurements revealed that the thickness of device #4, #5, and #6 is 105 ± 2, 320 ± 2, and 205 ± 2 nm, respectively. When Se concentration is 20 ± 5%, $R(T)$ shows an insulating behavior, but it saturates below ∼75 K due to the metallic surface transport as well as the bulk impurity-band transport.[25,26] The nonmetallic R *vs* T observed in these nanoribbons is consistent with those reported in the bulk crystals of $Bi_{2-x}Sb_xTe_{3-y}Se_y$,[25,26] and similar nonmetallic properties were also observed in Na-doped Bi_2Te_3 nanoplates and $Bi_2(Se_xTe_{1-x})_3$ nanoribbons/plates.[28,30]

Since the topological surface states are gapless, ambipolar conduction in the gate voltage tuned devices is taken as a signature of TI surface transport.[16,17,27] For $Bi_2(Te_{1-x}Se_x)_3$ nanoribbons or Bi_2Te_2Se nanoplates, either very high electron density was observed[30] or only the n-type conduction was achieved in the gating experiment, meaning the Fermi level was still

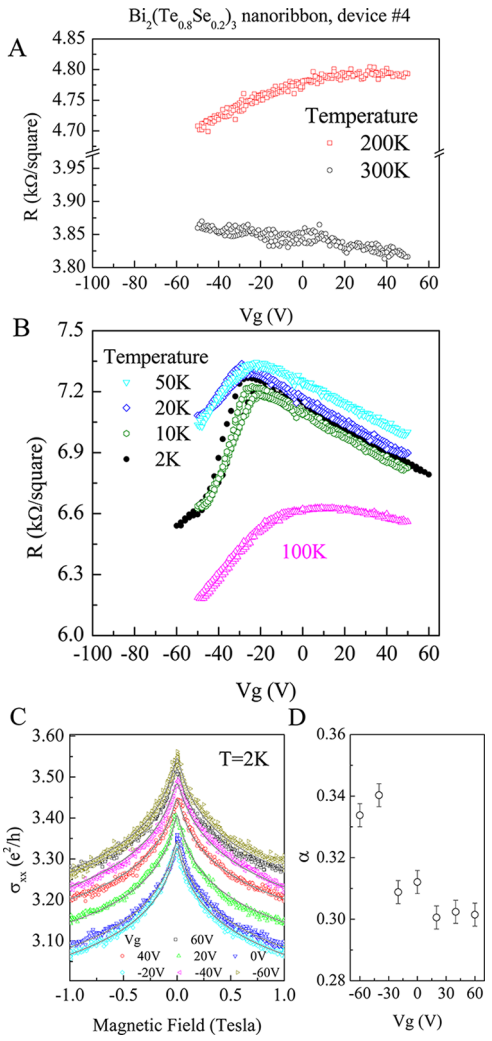

Figure 3. Gate voltage tuned ambipolar surface conduction and weak antilocalization in a $Bi_2(Te_{0.8}Se_{0.2})_3$ nanoribbon. (A, B) Dependence of resistance per square *vs* gate voltage at different temperatures for a 105 nm thick $Bi_2(Te_{0.8}Se_{0.2})_3$ nanoribbon (device #4), which shows ambipolar behavior at T < 200 K. (C) Magneto-conductivity of the device at different gate voltage, showing weak antilocalization effect. The symbols are data, and solid lines are fits. (D) Fitting parameter α in the weak antilocalization fit *vs* gate voltage.

above the Dirac point.[31] In our experiments, we found that with the bulk carrier conduction suppressed by the incorporation of Se, nanoribbons of ternary $Bi_2(Te_{1-x}Se_x)_3$ could start to exhibit ambipolar field effect in samples with thicknesses ∼100 nm or even larger. Figure 3A,B shows the zero-field resistance as a function of the back-gate voltage (V_g) at various temperatures for device #4, where x is ∼20% and the sample thickness is ∼105 nm. It is interesting to note that the gate-modulated resistance showed distinct behaviors at different temperatures. At 300 K, the resistance increased with decreasing the gate voltage, exhibiting a clear n-type feature. When the temperature was decreased to 200 K, the device kept a weak n-type characteristic with high gate voltage; however the resistance started to decrease when the applied gate voltage was

below about +20 V. This behavior indicates a transition from n-type to p-type conduction. When the temperature dropped further down to 2 K, an ambipolar characteristic became more evident in the $R(V_g)$ curve and the turning point moved to ~−20 V, as shown in Figure 3B. This behavior in the temperature effect on the ambipolar field effect can be understood by considering the relative contributions from surface and bulk states at different T: since the semiconducting $R(T)$ of $Bi_2(Te_{0.8}Se_{0.2})_3$ samples in Figure 2 suggests that the Fermi level resides in the bulk band gap in these samples, there are exponentially more thermally excited electrons in the bulk at high temperatures, which may smear out the ambipolar field effect from the gapless surface states. Further studies on the gate-tuned Hall resistivity at different temperatures would be required to quantitatively distinguish the surface carrier density and mobility from the bulk states by a multiband transport analysis, as previously done on bulk or exfoliated flakes of topological insulator materials.[17,21,22,32] Unfortunately, making Hall measurements has been difficult for our nanowires/nanoribbons. Such measurement and analysis will be a subject of future study.

In addition to ambipolar field effect, we observed that a 2D weak antilocalization effect also evolves with the gate voltage. Figure 3c shows the conductivity σ_{xx} in units of e^2/h *versus* perpendicular magnetic field (B) at 2 K at various V_g. The sharply peaked behavior near $B = 0$ indicates a weak antilocalization effect. We fit the conductivity data to the 2D weak antilocalization model $\Delta\sigma_{xx} = \alpha e^2/(2\pi^2\hbar)[\ln(B_\varphi/B) - \psi(1/2 + (B_\varphi/B))]$, where $B_\varphi = \hbar/(4eL_\varphi^2)$ is a characteristic field defined by the dephasing length L_φ, ψ is the digamma function, and α is a constant.[17,18,33] Correlating with the crossover from n- to p-type conduction at $V_g \approx -20$ V, we observe that α increases as V_g becomes smaller than −20 V. Previous measurements on molecular beam epitaxy grown Bi_2Se_3 thin films with a thickness of 20 nm or thinner showed that α increased from ~0.5 or 0.7 toward 1, concomitant with the ambipolar field effect in the gate-tuned conductance.[18,33] It is known that both conventional 2D films with strong spin−orbit coupling and a single layer of TI surface can contribute a weak antilocalization correction with α = 1/2. So this gate-tuned change of α from 0.5 to 1 was attributed to the gate-induced separation of bulk states from surface states when one of the TI surfaces was gated to the Dirac point, leaving the bulk states and the top TI surface, each contributing 0.5 to the total α.[18,33] Although we have obtained a similar increasing trend of α at $V_g < -20$ V accompanying the ambipolar conduction, the magnitude of enhancement in α is smaller and α itself (~0.3−0.34) is smaller than 0.5. This discrepancy in the quantitative magnitude of α may lie in the fact that for our sample the conductivity σ_{xx} is only 3−4 e^2/h. Strictly speaking, the weak antilocalization fitting only works in the diffusive metallic transport regime where

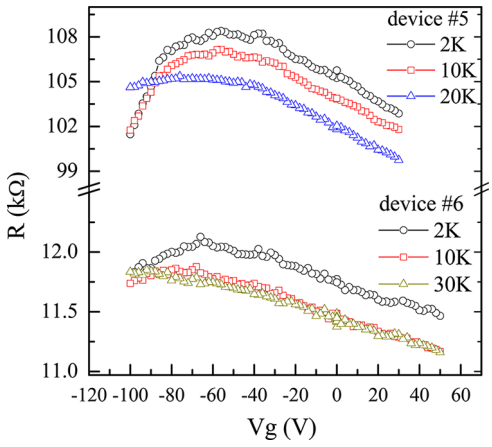

Figure 4. Ambipolar conduction in $Bi_2(Te_{1-x}Se_x)_3$ nanoribbons with large thickness. Gate voltage tuned ambipolar conduction at various temperatures in $Bi_2(Te_{1-x}Se_x)_3$ nanoribbons with $x \approx 0.2$ and thicknesses of about 205 nm (device #5) and 320 nm (device #6).

$\sigma_{xx} \gg e^2/h$. For σ_{xx} comparable to quantum conductance e^2/h, it is reasonable to expect that the standard weak antilocalization model does not give a quantitatively accurate fitting result, although it captures the qualitative physics.

It is remarkable that a clear ambipolar field effect is observed in nanoribbons with a thickness of ~100 nm, attesting to the effectiveness of including Se to compensate the defect states in Bi_2Te_3 to achieve an insulating bulk behavior. Previously, gate voltage induced ambipolar conduction was observed in Bi_2Se_3 flakes or films with thicknesses less than 50 nm.[16−18,24] In $(Bi_xSb_{1-x})_2Te_3$ nanoplates, the ambipolar field effect was very weak once the plate thickness increased above 9 nm.[27] Indeed, comparing our $Bi_2(Se_xTe_{1-x})_3$ nanoribbons with the same x but different thickness, we found thicker samples exhibited a weaker ambipolar field effect, due to the more dominant bulk contribution to the overall conductance. For 105 nm thick device #4, the ambipolar effect can be clearly seen even at 100 K, as shown in Figure 3B. But for thicker nanoribbon devices #5 (thickness ~205 nm) and #6 (thickness ~320 nm), the dependence of R on V_g shows a weaker tunability, as shown in Figure 4. Moreover, the ambipolar surface conduction effect disappeared at 20 and 10 K for devices #5 and #6, respectively. In addition, it is noted that the gate voltage for the transition from n- to p-type conduction is about −20 V for 105 nm thick device #4. However, with the thickness increased, this gate voltage is increased to about −60 and −70 V for device #5 and device #6. Therefore, it is important to fabricate devices with small thickness to enhance the ratio between surface conductance and bulk conductance for better characterization of topological surface transport.

CONCLUSION

In summary, we realized efficient suppression of bulk carrier transport in $Bi_2(Se_xTe_{1-x})_3$ nanoribbons/

nanowires with increasing Se concentration x. Semiconducting temperature-dependent resistivity was observed in $Bi_2(Se_xTe_{1-x})_3$ nanoribbons/nanowires with thicknesses of 100−300 nm at $x \approx 20\%$, indicating that the Fermi level was tuned into the bulk band gap. Moreover, as a result of reduced bulk conduction, an ambipolar field effect from the gapless surface states was observed in $Bi_2(Se_{0.8}Te_{0.2})_3$ nanoribbons/nanowires with thicknesses greater than 100 nm. This study illustrates the usefulness of composition-tuned ternary topological insulator nanomaterials in transport studies of topological insulators.

METHODS

The VLS growth method was used to synthesize ternary $Bi_2(Te_{1-x}Se_x)_3$ nanoribbons, using 20 nm gold nanoparticles (Ted Pella, Inc.) as metal catalyst on Si substrates. Pure Bi_2Te_3 and Bi_2Se_3 powders (99.999%, Alfa Aesar) were used as precursor. Bi_2Te_3 was placed in the center of a one inch diameter quartz tube inside a furnace (Lindberg/Blue M), and Bi_2Se_3 was placed at different sites far from the center in a low-temperature area. The atomic ratio of Te/Se in these nanoribbons was controlled by changing the distance of Bi_2Te_3 and Bi_2Se_3 precursors. The growth conditions for $Bi_2(Te_{1-x}Se_x)_3$ nanoribbons were similar to the conditions for Bi_2Se_3 nanoribbons.[14] The concentrations of Bi, Te, and Se in $Bi_2(Te_{1-x}Se_x)_3$ nanoribbons were estimated by EDS equipped in a Hitachi S4500 SEM. Back-gated $Bi_2(Te_{1-x}Se_x)_3$ nanoribbon FET devices were fabricated by standard photolithography patterning and liftoff processes, with doped Si wafers as substrates. The Si substrates had 300 nm thick SiO_2 on the surface as a gate dielectric. The transport properties of $Bi_2(Te_{1-x}Se_x)_3$ nanoribbon devices were measured in a Quantum Design PPMS (physical property measurement system) using low-frequency lock-in technique. The resistance (R) was measured in either a four-probe[14] or two-probe configuration. We found that the contact resistance was small, and the four-probe measurement gave a result similar to that of a simple two-probe configuration.

Conflict of Interest: The authors declare no competing financial interest.

Acknowledgment. Z.H.W. acknowledges China Scholarship Council for a scholarship supporting her visit to CWRU. X.P.A.G. acknowledges the NSF CAREER Award program (Grant No. DMR-1151534) for financial support of research at CWRU. Z.D. Z. acknowledges the National Natural Science Foundation of China for Grant No. 50831006.

REFERENCES AND NOTES

1. Hasan, M. Z.; Kane, C. L. Colloquium: Topological insulators. *Rev. Mod. Phys.* **2010**, *82*, 3045–3067.
2. Moore, J. E. The Birth of Topological Insulators. *Nature* **2010**, *464*, 194–198.
3. Zhang, H.; Liu, C. X.; Qi, X. L.; Dai, X.; Fang, Z.; Zhang, S. C. Topological Insulators in Bi_2Se_3, Bi_2Te_3 and Sb_2Te_3 with a Single Dirac Cone on the Surface. *Nat. Phys.* **2009**, *5*, 438–442.
4. Xia, Y.; Qian, D.; Hsieh, D.; Wray, L.; Pal, A.; Lin, H.; Bansil, A.; Grauer, D.; Hor, Y. S.; Cava, R. J.; *et al.* Observation of a Large-Gap Topological-Insulator Class with a Single Dirac Cone on the Surface. *Nat. Phys.* **2009**, *5*, 398–402.
5. Chen, Y. L.; Analytis, J. G.; Chu, J. H.; Liu, Z. K.; Mo, S. K.; Qi, X. L.; Zhang, H. J.; Lu, D. H.; Dai, X.; Fang, Z.; *et al.* Experimental Realization of a Three-Dimensional Topological Insulator, Bi_2Te_3. *Science* **2009**, *325*, 178–181.
6. Hsieh, D.; Xia, Y.; Qian, D.; Wray, L.; Meier, F.; Dil, J. H.; Osterwalder, J.; Patthey, L.; Fedorov, A. V.; Lin, H.; *et al.* Observation of Time-Reversal-Protected Single-Dirac-Cone Topological-Insulator States in Bi_2Te_3 and Sb_2Te_3. *Phys. Rev. Lett.* **2009**, *103*, 146401.
7. Chen, Y. L.; Chu, J. H.; Analytis, J. G.; Liu, Z. K.; Igarashi, K.; Kuo, H. H.; Qi, X. L.; Mo, S. K.; Moore, R. G.; Lu, D. H.; *et al.* Massive Dirac Fermion on the Surface of a Magnetically Doped Topological Insulator. *Science* **2010**, *329*, 659–662.
8. Alpichshev, Z.; Analytis, J. G.; Chu, J. H.; Fisher, I. R.; Chen, Y. L.; Shen, Z. X.; Fang, A.; Kapitulnik, A. STM Imaging of Electronic Waves on the Surface of Bi_2Te_3: Topologically Protected Surface States and Hexagonal Warping Effects. *Phys. Rev. Lett.* **2010**, *104*, 016401.
9. Zhang, Y.; He, K.; Chang, C. Z.; Song, C. L.; Wang, L. L.; Chen, X.; Jia, J. F.; Fang, Z.; Dai, X.; Shan, W. Y.; *et al.* Crossover of the Three-Dimensional Topological Insulator Bi_2Se_3 to the Two-Dimensional Limit. *Nat. Phys.* **2010**, *6*, 584–588.
10. Analytis, J. G.; McDonald, R. D.; Riggs, S. C.; Chu, J. H.; Boebinger, G. S.; Fisher, I. R. Two-Dimensional Surface State in the Quantum Limit of a Topological Insulator. *Nat. Phys.* **2010**, *6*, 960–964.
11. Peng, H.; Lai, K. J.; Kong, D. S.; Meister, S.; Chen, Y. L.; Qi, X. L.; Zhang, S. C.; Shen, Z. X.; Ciu, Y. Aharonov−Bohm Interference in Topological Insulator Nanoribbons. *Nat. Mater.* **2010**, *9*, 225–229.
12. Qu, D. X.; Hor, Y. S.; Xiong, J.; Cava, R. J.; Ong, N. P. Quantum Oscillations and Hall Anomaly of Surface States in the Topological Insulator Bi_2Te_3. *Science* **2010**, *329*, 821–824.
13. Xiu, F.; He, L.; Wang, Y.; Cheng, L.; Chang, L. T.; Lang, M.; Huang, G.; Kou, X.; Zhou, Y.; Jiang, X.; *et al.* Manipulating Surface States in Topological Insulator Nanoribbons. *Nat. Nanotechnol.* **2011**, *6*, 216–221.
14. Tang, H.; Liang, D.; Richard, Qiu L. J.; Gao, P. A. X. Two-Dimensional Transport-Induced Linear Magneto-Resistance in Topological Insulator Bi_2Se_3 Nanoribbons. *ACS Nano* **2011**, *5*, 7510–7516.
15. Chen, J.; Qin, H. J.; Liu, J.; Guan, T.; Qu, M F.; Zhang, G. H.; Shi, J. R.; Xie, X. C.; Yang, C. L.; Wu, K. H.; *et al.* Gate-Voltage Control of Chemical Potential and Weak Antilocalization in Bi_2Se_3. *Phys. Rev. Lett.* **2010**, *105*, 176602.
16. Checkelsky, J. G.; Hor, Y. S.; Cava, R. J.; Ong, N. P. Bulk Band Gap and Surface State Conduction Observed in Voltage-Tuned Crystals of the Topological Insulator Bi_2Se_3. *Phys. Rev. Lett.* **2011**, *106*, 196801.
17. Steinberg, H.; Gardner, D. R.; Lee, Y. S.; Jarillo-Herrero, P. Surface State Transport and Ambipolar Electric Field Effect in Bi_2Se_3 Nanodevices. *Nano Lett.* **2010**, *10*, 5032–5036.
18. Steinberg, H.; Laloe, J. B.; Fatemi, V.; Moodera, J. S.; Jarllo-Herrero, P. Electrically Tunable Surface-to-Bulk Coherent Coupling in Topological Insulator Thin Films. *Phys. Rev. B* **2011**, *84*, 233101.
19. Analytis, J. G.; Chu, J. H.; Chen, Y.; Corredor, F.; McDonald, R. D.; Shen, Z. X.; Fisher, I. R. Bulk Fermi Surface Coexistence with Dirac Surface State in Bi_2Se_3: A Comparison of Photoemission and Shubnikov−de Haas Measurements. *Phys. Rev. B* **2010**, *81*, 205407.
20. Kong, D. S.; Cha, J. J.; Lai, K.; Peng, H.; Analytis, J. G.; Meister, S.; Chen, Y.; Zhang, H. J.; Fisher, I. R.; Shen, Z. X.; *et al.* Rapid Surface Oxidation as a Source of Surface Degradation Factor for Bi_2Se_3. *ACS Nano* **2011**, *5*, 4698–4703.
21. Ren, Z.; Taskin, A. A.; Sasaki, S.; Segawa, K.; Ando, Y. Observations of Two-Dimensional Quantum Oscillations and Ambipolar Transport in the Topological Insulator Bi_2Se_3 Achieved by Cd Doping. *Phys. Rev. B* **2011**, *84*, 075316.
22. Ren, Z.; Taskin, A. A.; Sasaki, S.; Segawa, K.; Ando, Y. Large Bulk Resistivity and Surface Quantum Oscillations in the Topological Insulator Bi_2Te_2Se. *Phys. Rev. B* **2010**, *82*, 241306(R).
23. Gehring, P.; Gao, Bo F.; Burghard, M.; Kern, K. Growth of High-Mobility Bi_2Te_2Se Nanoplatelets on hBN Sheets by van der Waals Epitaxy. *Nano Lett.* **2012**, *12*, 5137–5142.

24. Checkelsky, J. G.; Hor, Y. S.; Liu, M. H.; Qu, D. X.; Cava, R. J.; Ong, N. P. Quantum Interference in Macroscopic Crystals of Nonmetallic Bi_2Se_3. *Phys. Rev. Lett.* **2009**, *103*, 246601.
25. Ren, Z.; Taskin, A. A.; Sasaki, S.; Segawa, K.; Ando, Y. Optimizing $Bi_{2-x}Sb_xTe_{3-y}Se_y$ Solid Solutions to Approach the Intrinsic Topological Insulator Regime. *Phys. Rev. B* **2011**, *84*, 165311.
26. Taskin, A. A.; Ren, Z.; Sasaki, S.; Segawa, K.; Ando, Y. Observation of Dirac Holes and Electrons in a Topological Insulator. *Phys. Rev. Lett.* **2011**, *107*, 016801.
27. Kong, D. S.; Chen, Y. L.; Cha, J. J.; Zhang, Q. F.; Analytis, J. G.; Lai, K. J.; Liu, Z. K.; Hong, S. S.; Koski, K. J.; Mo, S. K.; *et al*. Ambipolar Field Effect in the Ternary Topological Insulator $(Bi_xSb_{1-x})_2Te_3$ by Composition Tuning. *Nat. Nanotechnol.* **2011**, *6*, 705–709.
28. Wang, Y.; Xiu, F.; Cheng, L.; He, L.; Lang, M.; Tang, J. S.; Kou, X. F.; Yu, X. X.; Jiang, X. W.; Chen, Z. G.; *et al*. Gate-Controlled Surface Conduction in Na-Doped Bi_2Te_3 Topological Insulator Nanoplates. *Nano Lett.* **2012**, *12*, 1170–1175.
29. Zhang, J.; Chang, C. Z.; Zhang, Z.; Wen, J.; Feng, X.; Li, K.; Liu, M.; He, K.; Wang, L.; Chen, X.; *et al*. Band Structure Engineering in $(Bi_{1-x}Sb_x)_2Te_3$ Ternary Topological Insulators. *Nat. Commun.* **2011**, *2*, 574.
30. Cha, J. J.; Kong, D. S.; Hong, S. S.; Analytis, J. G.; Lai, K.; Cui, Y. Weak Antilocalization in $Bi_2(Se_xTe_{1-x})_3$ Nanoribbons and Nanoplates. *Nano Lett.* **2012**, *12*, 1107–1111.
31. Gehring, P.; Gao, B.; Burghard, M.; Kern, K. Two-Dimensional Magnetotransport in Bi_2Te_2Se Nanoplatelets. *Appl. Phys. Lett.* **2012**, *101*, 023116.
32. Lee, J.; Park, J.; Lee, J.-H.; Kim, J. S.; Lee, H.-J. Gate-Tuned Differentiation of Surface-Conducting States in $Bi_{1.5}Sb_{0.5}Te_{1.7}Se_{1.3}$ Topological-Insulator Thin Crystals. *Phys. Rev. B* **2012**, *86*, 245321.
33. Chen, J.; He, X. Y.; Wu, K. H.; Ji, Z. Q.; Lu, L.; Shi, J. R.; Smet, J. H.; Li, Y. Q. Tunable Surface Conductivity in Bi_2Se_3 Revealed in Diffusive Electron Transport. *Phys. Rev. B* **2011**, *83*, 241304(R).